NASA
Technical Memorandum 105765

AVSCOM
Technical Report 91–C–046

In-Phase and Out-of-Phase Axial-Torsional Fatigue Behavior of Haynes 188 at 760 °C

Sreeramesh Kalluri
Sverdrup Technology, Inc.
Lewis Research Center Group
Brook Park, Ohio

and

Peter J. Bonacuse
Propulsion Directorate
U.S. Army Aviation Systems Command
Lewis Research Center
Cleveland, Ohio

Prepared for the
Symposium on Multiaxial Fatigue
sponsored by the American Society for Testing and Materials
San Diego, California, October 14–15, 1991

NASA

US ARMY
AVIATION
SYSTEMS COMMAND

IN-PHASE AND OUT-OF-PHASE AXIAL-TORSIONAL FATIGUE BEHAVIOR OF HAYNES 188 AT 760 °C

Sreeramesh Kalluri
Sverdrup Technology, Inc.
Lewis Research Center Group
Brook Park, Ohio 44142

and

Peter J. Bonacuse
Propulsion Directorate
U.S. Army Aviation Systems Command
Lewis Research Center
Cleveland, Ohio 44135

E-7182

SUMMARY

Isothermal, in-phase and out-of-phase axial-torsional fatigue experiments have been conducted at 760 °C on uniform gage section, thin-walled tubular specimens of a wrought cobalt-base superalloy, Haynes 188. Test-control and data acquisition were accomplished with a minicomputer. Fatigue lives of the in- and out-of-phase axial-torsional fatigue tests have been estimated with four different multiaxial fatigue life prediction models that were developed primarily for predicting axial-torsional fatigue lives at room temperature. The models investigated were: (1) the von Mises equivalent strain range, (2) the Modified Multiaxiality Factor Approach, (3) the Modified Smith-Watson-Topper Parameter, and (4) the critical shear plane method of Fatemi, Socie, and Kurath. In general, life predictions by the von Mises equivalent strain range model were within a factor of 2 for a majority of the tests and the predictions by the Modified Multiaxiality Factor Approach were within a factor of 2, while predictions of the Modified Smith-Watson-Topper Parameter and of the critical shear plane method of Fatemi, Socie, and Kurath were unconservative and conservative, respectively, by up to factors of 4. In some of the specimens tested under combined axial-torsional loading conditions, fatigue cracks initiated near extensometer indentations. Two design modifications have been proposed to the thin-walled tubular specimen to overcome this problem.

INTRODUCTION

Fatigue lives under cyclic multiaxial loading conditions can differ significantly from those observed under "equivalent" cyclic uniaxial loading conditions. This can be attributed to the additional damage and deformation mechanisms that are activated under multiaxial loading conditions (refs. 1 to 4). In order to develop and verify multiaxial fatigue life prediction models, it is imperative that fatigue tests be conducted under multiaxial loading conditions. Thin-walled tubular specimens are commonly used to investigate the fatigue behavior of engineering alloys under combinations of (1) axial and torsional, (2) axial and internal/external pressure, and (3) axial, torsional, and internal/external pressure loading conditions.

Numerous investigations have been conducted over the last two decades on thin-walled tubular specimens to characterize the fatigue behavior of several engineering alloys under combined axial and torsional loading conditions (refs. 5 to 19). These investigations involved both in-phase, $\phi = 0°$ (refs. 5 to 19), and out-of-phase, $\phi \neq 0°$ (refs. 5, 7, 8, 11 to 17, and 19), strain-controlled, axial-torsional fatigue

tests and were performed with various values of λ, (refs. 5 to 7, 10, and 13 to 17). The types of engineering alloys studied included an aluminum alloy (ref. 5), low alloy steels (refs. 7, 11, and 13 to 15), stainless steels (refs. 6, 10 to 12, 16, 18, and 19), and nickel-base superalloys (refs. 8, 9, 11, 13, 14, and 17). A great many of these investigations were conducted at room temperature (refs. 5 to 15 and 17 to 19) with only a few studies conducted at elevated temperatures (refs. 6 and 16). This can be primarily attributed to the added complexity of performing axial-torsional fatigue tests at elevated temperatures. However, the development of minicomputers during the last decade, and the subsequent application of these minicomputers to fatigue test control and data acquisition have reduced the difficulties in conducting elevated temperature axial-torsional fatigue tests.

In this study, fatigue behavior of a wrought cobalt-base superalloy, Haynes 188, has been investigated at 760 °C by subjecting thin-walled tubular specimens to combined cyclic axial and torsional loads. Strain-controlled, in-phase as well as out-of-phase axial-torsional fatigue tests have been conducted, in air, with different proportionality constants. Fatigue lives of the elevated temperature in- and out-of-phase axial-torsional tests have been estimated with four different multiaxial fatigue life prediction models. A majority of these models were originally developed for room temperature applications. Constants for the multiaxial fatigue life prediction models were obtained from previously generated axial and torsional fatigue data of Haynes 188 (ref. 20). Fatigue crack initiation occurred near the extensometer indentations in some of the specimens tested under combined axial and torsional loads. To alleviate this problem, it is proposed that either an hourglass or a straight section detail be machined within the uniform gage section of the thin-walled tubular test specimen.

NOMENCLATURE

B,C	coefficients of axial elastic and plastic strain range-life relations
B_t,C_t	coefficients of torsional elastic and plastic strain range-life relations
b,c	exponents of axial elastic and plastic strain range-life relations
b_t,c_t	exponents of torsional elastic and plastic strain range-life relations
E,G	Young's and shear moduli
K,K'	monotonic and cyclic axial strength coefficients
K_t,K'_t	monotonic and cyclic torsional strength coefficients
k	constant in Fatemi-Socie-Kurath Parameter
MF,TF	multiaxiality and triaxiality factors
N_f	cycles to failure
n,n'	monotonic and cyclic axial strain hardening exponents
n_t,n'_t	monotonic and cyclic torsional strain hardening exponents
%RA	percent reduction in area

γ,ε	engineering shear and axial strain amplitudes
γ_f',ε_f'	torsional and axial fatigue ductility coefficients, $C_t/2^{(1+c_t)}$ & $C/2^{(1+c)}$
γ_{max}	maximum engineering shear strain amplitude
$\gamma_{xy},\gamma_{yz},\gamma_{zx}$	orthogonal engineering shear strains
Δ	denotes range of the variable
ε_1	first principal strain amplitude
ε_e, ε_p	axial elastic and plastic strain amplitudes
ε_{eq}	von Mises equivalent strain amplitude
$\varepsilon_{xx},\varepsilon_{yy},\varepsilon_{zz}$	orthogonal normal strains
λ	proportionality constant, γ/ε
ν_e, ν_p	elastic and plastic Poisson's ratios
ν_{eff}	effective Poisson's ratio
σ, τ	axial and shear stress amplitudes
σ_o, τ_o	mean axial and shear stresses
$\sigma_1,\sigma_2,\sigma_3$	principal stresses
σ_1^{max}	maximum stress on the maximum principal strain plane
σ_f', τ_f'	axial and torsional fatigue strength coefficients, $BE/2^{(1+b)}$ & $B_tG/2^{(1+b_t)}$
σ_n^{max}	maximum normal stress on the maximum shear strain plane
σ_y, τ_y	axial and shear yield strengths
σ_u	ultimate tensile strength
ϕ	phase angle between axial and engineering shear strain waveforms

MATERIAL DESCRIPTION

The wrought cobalt-base superalloy, Haynes 188, was supplied by a commercial vendor in the form of hot rolled, solution-annealed, round bars with a nominal diameter of 50.8 mm. The chemical composition of the superalloy in weight percent is as follows: <0.002 S; 0.002 B; 0.012 P; 0.1 C; 0.4 Si; 0.034 La; 0.75 Mn; 1.24 Fe; 13.95 W; 21.84 Cr; 22.43 Ni; and the balance is cobalt. The grain size of the supplied material ranges from 45 to 65 μm.

EXPERIMENTAL DETAILS

Test Specimen

All the fatigue data and properties presented in this paper have been generated by using uniform gage section, thin-walled, tubular specimens (fig. 1) that were fabricated from a single heat of Haynes 188. The outer surface of each tubular specimen was polished such that the final polishing marks were parallel to the longitudinal axis of the specimen. The cylindrical bore of each specimen was finished with a honing operation to inhibit fatigue crack initiation from the inner surface. The prescribed surface roughness average values for the inner and outer surfaces of the tubular specimen were 0.2 and 0.4 μm, respectively.

Test System and Extensometer

All the fatigue tests were conducted on a servohydraulic axial-torsional fatigue system. A commercial high temperature extensometer was used to measure and control axial and engineering shear strains. Two indentations were pressed into the outer surface (within the uniform section) of the thin-walled tubular specimen with a fixture that allowed the indentation force to be precisely controlled. These indentations were 25 mm apart and were used to mount the quartz probes of the extensometer on the specimen. The indentations prevented slippage of the extensometer during a fatigue test. Additional details on the fatigue rig and extensometer are available in references 18 and 21. The tubular specimens were inductively heated to the required test temperature. Chromel-alumel thermocouples, spot-welded just outside the gage section, were used to monitor and control the specimen temperature. Variation of temperature along the uniform section of the specimen was within 1 percent of the nominal test temperature. Additional details on the heating system and on the temperature profile determination are provided in reference 20.

Test Control and Data Acquisition

All in- and out-of-phase axial-torsional fatigue tests have been conducted at 760 °C in air, under strain control, and at a frequency of 0.1 Hz. Triangular waveforms with the required value of ϕ were generated to control axial and engineering shear strains. Computer software developed specifically for axial-torsional fatigue testing was used for dual waveform generation and data acquisition (ref. 21). In each fatigue test, cyclic stress-strain data were acquired at logarithmic intervals until failure of the specimen. Failure was defined as a 10 percent reduction in either the axial or the torsional peak load from the last recorded cycle.

FATIGUE DATABASE

Baseline Axial and Torsional Properties

Monotonic axial and torsional, axial fatigue ($\lambda = 0$), and torsional fatigue ($\lambda = \infty$) tests were conducted previously (ref. 20) on thin-walled tubular specimens of Haynes 188 (fig. 1) at 760 °C. In reference 20 a Ramberg-Osgood type stress-strain relation was used to describe the monotonic and cyclic stress-strain curves under axial and torsional conditions. These relations for the monotonic axial and engineering shear stress-strain curves are as follows:

$$\varepsilon = \frac{\sigma}{E} + \left[\frac{\sigma}{K}\right]^{1/n} \quad \text{for monotonic axial test}$$

or (1)

$$\gamma = \frac{\tau}{G} + \left[\frac{\tau}{K_t}\right]^{1/n_t} \quad \text{for monotonic torsional test}$$

The relations for cyclic axial and engineering shear stress-strain curves can be obtained by replacing n, n_t, K, and K_t in equation (1) by n', n_t', K', and K_t', respectively. The fatigue life relations used in reference 20 to describe the axial and torsional fatigue data are as follows:

$$\Delta\varepsilon = B(N_f)^b + C(N_f)^c \tag{2}$$

$$\Delta\gamma = B_t(N_f)^{b_t} + C_t(N_f)^{c_t} \tag{3}$$

Monotonic and cyclic, axial and engineering shear stress-strain properties, and axial and torsional fatigue properties (ref. 20) for Haynes 188 at 760 °C are listed in table I.

Combined Axial-Torsional Fatigue Data

In this program, in- and out-of-phase axial-torsional fatigue tests have been conducted at 760 °C on thin-walled tubular specimens of Haynes 188 (table II). In-phase fatigue tests ($\phi = 0°$) were conducted with nominal λ values of 0.86, 1.73, and 3.46. Out-of-phase tests were conducted with $\lambda = 1.73$ and $\phi = 30°$, 60°, and 90°. These test conditions were selected to cover a range of proportionality constants and phase angles for Haynes 188. Two out-of-phase fatigue tests ($\lambda = 1.73$ and $\phi = 90°$) have also been conducted with 0.1 Hz sinusoidal waveforms for axial and engineering shear strains to study the effect of waveform on fatigue life. The axial and shear stresses and axial and engineering shear strains reported in table II were obtained from near half-life hysteresis loops for all the tests. In all the in- and out-of-phase axial-torsional fatigue test specimens the fatigue crack that caused failure occurred nearly perpendicular to the maximum normal strain direction.

For similar values of controlled axial and engineering shear strain ranges, the out-of-phase tests exhibited significantly more hardening than the in-phase tests. For example, in table II, two specimens (HY26 and HY65) have been tested under similar axial and engineering shear strain ranges. Specimen HY65 tested under an out-of-phase loading condition ($\phi = 90°$) exhibited 44 percent more axial and 52 percent more torsional hardening than specimen HY26, which was tested under an in-phase loading condition ($\phi = 0°$).

For cyclic lives less than 6000, no significant difference was observed in the fatigue lives of in- and out-of-phase axial-torsional fatigue tests with similar values of the applied axial and engineering shear strains. However, for cyclic lives greater than 6000, the out-of-phase tests exhibited cyclic lives that were greater than the corresponding in-phase fatigue lives by factors of 1.5 to 3 or more (table II). The fatigue lives of specimens tested with the sinusoidal waveforms were slightly lower than those tested with triangular waveforms (HY38 & HY68 and HY56 & HY46 in table II). However, these fatigue lives were within a factor of 2 and the cyclic hardening under these two types of waveforms was almost identical.

There were two specimens, one in-phase test and one out-of-phase test, that did not fail and these tests have been classified as runouts.

Specimen failure in both the in- and out-of-phase axial-torsional fatigue tests (with the exception of one datum) was caused by a crack at an extensometer indentation whenever N_f exceeded 6000 cycles. In one out-of-phase test, HY66 in table II, specimen failure due to indentation cracking was observed at $N_f = 1088$. However, this specimen actually lasted slightly longer than another specimen, HY65 in table II, that did not crack at an indentation under the same loading condition. Failure of specimens due to a crack at the indentation was also observed in the case of axial ($\lambda = 0$) and torsional ($\lambda = \infty$) fatigue tests (ref. 20). However, the number of such specimens was relatively small compared with the in- and out-of-phase tests, and the data corresponding to those specimens were omitted in computing the axial and torsional fatigue properties listed in table I.

LIFE PREDICTION

Many life prediction models have been proposed to estimate fatigue life under combined cyclic axial-torsional loading conditions (refs. 1, 2, 5, 6, 9, 11, 13, 14, 16, 20, 22, and 23). Some of these models include parameters based on the von Mises equivalent strain range (refs. 2 and 22), the von Mises equivalent strain range modified with a multiaxiality factor (refs. 20 and 23), the principal strains and/or stresses (refs. 5 and 11), and on a combination of maximum shear strain and the normal stress and/or normal strain acting on the maximum shear plane (refs. 1, 6, 9, 11, 13, 14, and 16). Most of these fatigue life prediction models were verified with room temperature axial-torsional data. In this study, four models have been chosen, one from each of the above categories, to evaluate their applicability to the high temperature in- and out-of-phase axial-torsional fatigue data of Haynes 188.

The models investigated are (1) von Mises equivalent strain range (ref. 22), (2) Modified Multiaxiality Factor Approach (ref. 20), (3) Modified Smith-Watson-Topper Parameter (ref. 11), and (4) critical shear plane method of Fatemi, Socie, and Kurath (refs. 13 and 14). The first three models require only axial fatigue data to predict fatigue lives under combined axial-torsional loads whereas the fourth model requires both the axial and torsional fatigue data. The predictive capabilities of the same four models were previously investigated (ref. 20) with the elevated temperature torsional fatigue data of Haynes 188 at 760 °C. It was found in reference 20 that for estimating the torsional fatigue ($\lambda = \infty$) lives with the axial fatigue ($\lambda = 0$) properties of Haynes 188 at 760 °C, the von Mises equivalent strain range model was conservative by up to a factor of 3, predictions by the Modified Multiaxiality Factor Approach were within a factor of 2, while the Modified Smith Watson-Topper Parameter was unconservative by up to a factor of 6. The critical shear plane method of Fatemi, Socie, and Kurath correlated the axial ($\lambda = 0$) and torsional ($\lambda = \infty$) fatigue data to within a factor of 2.5.

In the following sections, brief descriptions of the models and their fatigue life predictive capabilities for the in- and out-of-phase axial-torsional fatigue tests of Haynes 188 are presented.

von Mises Equivalent Strain Range Model

This model reduces a given cycle of multiaxial strains to a uniaxial equivalent strain range as shown in equation (4) (refs. 2 and 22).

$$\Delta\varepsilon_{eq} = \frac{\left[(\Delta\varepsilon_{xx} - \Delta\varepsilon_{yy})^2 + (\Delta\varepsilon_{yy} - \Delta\varepsilon_{zz})^2 + (\Delta\varepsilon_{zz} - \Delta\varepsilon_{xx})^2 + \frac{3}{2}\left(\Delta\gamma_{xy}^2 + \Delta\gamma_{yz}^2 + \Delta\gamma_{zx}^2\right)\right]^{1/2}}{\sqrt{2}\,(1 + \nu_{eff})} \quad (4)$$

Implementation of this model requires knowledge of all six components of strain throughout the cycle (ref. 22). For the in- and out-of-phase tests, an extreme condition in the cycle, the time at which a maximum or a minimum of a strain component occurs is selected as the reference time for all the strain components. The range for each strain component (the difference between the strains at the reference time and the current time) is then computed at each point in time for that cycle. At each point in time the equivalent strain range is computed using equation (4). The maximum equivalent strain range computed over a cycle is then used in the axial fatigue life relation (eq. (2)) for life prediction. For each out-of-phase axial-torsional fatigue test, the equivalent strain range has been computed twice: Once with the maximum axial strain as the reference and a second time with the maximum engineering shear strain as the reference. The larger of the two values was used for fatigue life prediction. For a given cycle, ν_{eff} was computed with the following equation by using the near half-life axial hysteresis loop.

$$\nu_{eff} = \left[\frac{\Delta\varepsilon_e\nu_e + \Delta\varepsilon_p\nu_p}{\Delta\varepsilon}\right]$$

$$\text{where:} \quad \Delta\varepsilon_e = \Delta\sigma/E \quad (5)$$

$$\text{and:} \quad \Delta\varepsilon_p = \Delta\varepsilon - \Delta\varepsilon_e$$

The lives predicted by the von Mises equivalent strain range method are shown in figure 2 for the in- and out-of-phase axial-torsional fatigue tests. Data points corresponding to specimens that failed due to a crack at an extensometer indentation are marked with a slash (/). In general, the fatigue lives of the in-phase tests were underpredicted and lives of the out-of-phase tests were overpredicted by this model. However, with the exception of a few data points, the predicted fatigue lives of both the in- and out-of-phase tests were within a factor of 2 of the observed fatigue lives (fig. 3).

Modified Multiaxiality Factor Approach

Manson and Halford (ref. 23), in their discussion of the work by Blass and Zamrik (ref. 6), proposed a multiaxiality factor that was based on the triaxiality factor of Davis and Connelly (ref. 24) to account for the state of stress on the ductility of a material. The original proposal of Manson and Halford required that the von Mises equivalent inelastic strain range under multiaxial conditions be multiplied by the multiaxiality factor. Bonacuse and Kalluri (ref. 20) extended the approach to the total von Mises equivalent strain range as shown in the following equation.

$$\Delta\varepsilon_{eq} = \left(\frac{B}{MF^{b/c}}\right)(N_f)^b + \left(\frac{C}{MF}\right)(N_f)^c \quad (6)$$

where,

$$MF = \frac{1}{2 - TF} \quad ; \; TF \leq 1$$

$$MF = TF \quad ; \; TF \geq 1 \tag{7}$$

$$\text{and:} \quad TF = \frac{\sigma_1 + \sigma_2 + \sigma_3}{\frac{1}{\sqrt{2}}\sqrt{(\sigma_1 - \sigma_2)^2 + (\sigma_2 - \sigma_3)^2 + (\sigma_3 - \sigma_1)^2}}$$

In the case of combined axial-torsional loading, MF assumes values between 0.5 (torsional loading; TF = 0) and 1.0 (axial loading; TF = 1). For the in- and out-of-phase axial-torsional fatigue tests, the total equivalent von Mises strain range has been computed as described previously and the MF has been computed at the maximum axial strain and at the maximum engineering shear strain in the cycle. Note that for an in-phase test only one such computation is necessary. For an out-of-phase test the larger of the two computed values of the MF was used for life prediction (eq. (6)). Lower and upper bounds of predicted fatigue lives for this model were obtained with MF = 1.0 and MF = 0.5, respectively. Most of the in- and out-of-phase axial-torsional fatigue data were within the lower and upper bounds of life predicted by this model (fig. 4). Fatigue life predictions by this model were within a factor of 2 of the observed lives (fig. 5). Comparison of figures 3 and 5 shows that life predictions by the Modified Multiaxiality Factor Approach are better than those by the von Mises equivalent strain range model for in-phase tests ($\phi = 0°$) and for out-of-phase tests for which $\phi \neq 90°$. The life predictions by the Modified Multiaxiality Factor Approach do not show any improvement over the von Mises equivalent strain range model for out-of-phase tests with $\phi = 90°$ because MF is very nearly equal to one for these tests.

Modified Smith-Watson-Topper Parameter

Smith, Watson, and Topper (ref. 25) proposed a stress-strain function to account for the effect of mean stress on the fatigue life of metals. Socie (ref. 11) argued that larger stresses (due to the extra hardening) in out-of-phase axial-torsional loading would have an effect on fatigue life that is similar to the effect of tensile mean stress on axial fatigue life and extended usage of the Smith-Watson-Topper parameter to axial-torsional fatigue life prediction.

$$\frac{\Delta\epsilon_1}{2}\,\sigma_1^{max} = \sigma_f'\,\epsilon_f'\,(2N_f)^{b+c} + \frac{\sigma_f'^2}{E}(2N_f)^{2b} \tag{8}$$

The Modified Smith-Watson-Topper Parameter was successfully used to predict the room temperature fatigue life under in- and out-of-phase axial-torsional loading conditions for materials that crack in a tensile mode, i.e., cracks initiate and propagate perpendicular to the maximum principal strain direction (refs. 11 and 12). In this model, the magnitude and the plane of the maximum principal strain amplitude is determined first for a given cycle of axial-torsional loading. The maximum principal strain amplitude is then multiplied by the maximum normal stress that occurs on that plane. For the in- and out-of-phase axial-torsional fatigue tests on Haynes 188, which exhibited a tensile mode of cracking, life predictions by this model were unconservative by up to a factor of 4 with the largest deviations occurring for the out-of-phase tests (figs. 6 and 7). Other investigators have reported unconservative fatigue life predictions by the Modified Smith-Watson-Topper Parameter for materials that exhibit a shear mode of failure, i.e., initiation of cracks parallel to the maximum shear plane (ref. 14).

Critical Shear Plane Method of Fatemi, Socie, and Kurath

The importance of the plane of maximum shear for crack initiation in multiaxial fatigue loading was recognized by Brown and Miller (ref. 1), Blass and Zamrik (ref. 6), and Kanazawa et al. (ref. 7). Their work indicated that parameters based on the maximum shear strain and the normal strain acting on the plane of maximum shear strain should be considered for prediction of fatigue failure under multiaxial stress-strain conditions. Socie and his co-workers (refs. 9 and 11) proposed the addition of a normal stress term to the shear and normal strain terms. The critical shear plane method developed by Fatemi and Socie (ref. 13) and Fatemi and Kurath (ref. 14), considers the maximum shear strain and the normal stress on the plane of maximum shear strain:

$$\gamma_{max}\left(1 + k\,\frac{\sigma_n^{max}}{\sigma_y}\right) = (1 + \nu_e)\,\frac{\sigma_f'}{E}\,(2N_f)^b + \frac{k}{2}\,(1 + \nu_e)\,\frac{\sigma_f'^2}{E\sigma_y}\,(2N_f)^{2b} + (1 + \nu_p)\varepsilon_f'(2N_f)^c + \frac{k}{2}\,(1 + \nu_p)\varepsilon_f'\,\frac{\sigma_f'}{\sigma_y}\,(2N_f)^{b+c} \tag{9}$$

The Fatemi-Socie-Kurath model was successfully used to predict room temperature in- and out-of-phase axial-torsional fatigue lives for materials that exhibit a shear mode of failure (ref. 14). Application of this model to the in- and out-of-phase, axial-torsional, Haynes 188 fatigue data has yielded very conservative life predictions (fig. 8). The material property constant k (eq. (9)) was determined in reference 20 by using both the axial ($\lambda = 0$) and torsional ($\lambda = \infty$) fatigue data of Haynes 188 according to the procedure described by Fatemi and Kurath (ref. 14). The value of k was equal to 1.0 for the fatigue life regime of interest in this study (ref. 20). Life predictions by this method were conservative by up to a factor of 4 or more for the combined axial-torsional fatigue tests (fig. 9).

DISCUSSION

Cyclic Hardening

For Haynes 188 at 760 °C, as mentioned earlier, the out-of-phase axial-torsional fatigue tests exhibited more cyclic axial and torsional hardening than the corresponding in-phase tests. Similar hardening behavior was observed in out-of-phase axial-torsional tests for a low alloy steel (ref. 13), stainless steels (refs. 11, 12, 16, and 19), and a nickel-base superalloy (ref. 17). For Haynes 188 at 760 °C, the axial stress-strain curves exhibited less hardening under in-phase tests ($\lambda = 1.73$ and $\phi = 0°$) and more hardening in out-of-phase tests ($\lambda = 1.73$ and $\phi = 90°$) compared to the cyclic stress-strain curve obtained from axial fatigue tests ($\lambda = 0$). Similar behavior was observed even for the cyclic engineering shear stress-strain curves under these combined axial-torsional loading conditions. For out-of-phase tests with $\lambda = 1.73$ and $\phi = 90°$, both the triangular and sinusoidal waveform tests exhibited similar hardening behavior which implies that the wave shape effects at the test frequency of 0.1 Hz are not very significant.

Indentation Cracking

In this study thin-walled tubular specimens that exhibited cyclic lives greater than 6000 cycles under combined axial-torsional loads typically failed due to a crack at an extensometer indentation (table II). No such cracking was observed in previously conducted room temperature studies on 304 and 316 stainless steels even though the cyclic lives were as high as 37 000 cycles (refs. 18 and 19). This observation indicates that Haynes 188 at 760 °C is a notch sensitive material. Note from table II that indentation cracking occurred in 7 out of 12 out-of-phase axial-torsional tests whereas such a cracking occurred in only 2 out of the 10 in-phase tests. Also indentation cracking was noticed at a low cyclic life of 1088 in the out-of-phase tests whereas it was not noticed in the in-phase tests until a cyclic life of 6261. The additional hardening occurring in the out-of-phase axial-torsional fatigue tests may have increased the notch-sensitivity of the material, which may be the reason for the frequent and early occurrence of indentation cracking under out-of-phase loading conditions compared to the in-phase loading conditions.

As mentioned earlier, between the two out-of-phase axial-torsional tests that had similar loading conditions (HY65 and HY66 in table II), the test that exhibited cracking at the indentation (HY66 with $N_f = 1088$) actually lasted slightly longer than the one that did not crack at an indentation (HY65 with $N_f = 944$). Thus, the effect of indentation cracking on the observed fatigue lives may not be very large. In any case, the life predictions by the four models used in the study are valid because they were based on cyclic life data from those axial and torsional fatigue tests, which did not exhibit any indentation cracking (ref. 20). In the absence of indentation cracking, if the fatigue lives of the specimens that exhibited indentation cracking were to increase, the life predictions by the von Mises equivalent strain range model and the Modified Multiaxiality Factor Approach would be conservative, the life predictions by the Modified Smith-Watson-Topper Parameter would be less unconservative, and the predictions by the Fatemi-Socie-Kurath model would be more conservative compared to the respective model predictions shown in figures 2 to 9.

Alternative Tubular Specimen Designs

Design of the thin-walled tubular specimen can be modified for notch-sensitive materials to prevent cracking at extensometer indentations. The modifications proposed involve machining of either a uniform cylindrical detail (fig. 10) or an hourglass cylindrical detail (fig. 11) within the gage section of the specimen. The indentations for mounting the extensometer would be pressed outside the cylindrical details in both of these designs. These designs greatly reduce the chances of cracking at the indentations because the highly stressed region is confined to the center of the tubular specimen and is removed from the indentations. However, these modified designs require additional computations, which are not required for the uniform gage section design (fig. 1), to estimate the strains at the minimum section of the specimen. In addition to the extra machining that is required, either of the proposed cylindrical details may introduce a temperature gradient within the gage section. Specimen designs containing similar cylindrical details have been used for multiaxial fatigue testing. Some of these thin-walled tubular specimen designs were summarized by Lefebvre (ref. 26).

CONCLUSIONS

In-phase and out-of-phase axial-torsional fatigue tests have been conducted at 760 °C on thin-walled tubular specimens fabricated from a wrought cobalt-base superalloy, Haynes 188. In-phase fatigue tests with nominal engineering shear to axial strain ratios of 0.87, 1.73, 3.46 and out-of-phase fatigue tests with a nominal engineering shear to axial strain ratio of 1.73 and with phase angles of 30°, 60°, and 90° have

been conducted. The fatigue lives of the in- and out-of-phase axial-torsional tests were estimated with four multiaxial life prediction models and the predicted cyclic lives were compared with the observed cyclic lives. The following conclusions were drawn from this study.

1. More cyclic axial and torsional hardening occurred under out-of-phase axial-torsional loading conditions than under in-phase axial-torsional loading conditions for Haynes 188.

2. Some of the thin-walled tubular specimens of Haynes 188 tested under combined axial-torsional loads failed due to a crack at an extensometer indentation. The number of such specimens was greater in the out-of-phase tests than in the in-phase tests. This phenomenon, in general, was attributed to the notch sensitivity of Haynes 188 at 760 °C. The additional hardening that occurred in the out-of-phase tests might have increased the degree of notch sensitivity of the material.

3. For cyclic lives less than 6000 (when compared on the basis of applied axial and engineering shear strain ranges) no significant difference was observed between the fatigue lives of in- and out-of-phase axial-torsional tests, while for cyclic lives greater than 6000 cycles, out-of-phase tests lasted factors of 1.5 to 3 or more longer than the in-phase tests.

4. Fatigue life predictions of the in-phase and out-of-phase axial-torsional tests were: (1) within a factor of 2 for a majority of tests for the von Mises equivalent strain range model, (2) within a factor of 2 for the Modified Multiaxiality Factor Approach, (3) unconservative by up to a factor of 4 for the Modified Smith-Watson-Topper Parameter, and (4) conservative by up to a factor of 4 for the Fatemi-Socie-Kurath Model.

5. Two design modifications were proposed to prevent specimen failure due to a crack at an extensometer indentation. These modifications add either a uniform cylindrical detail or an hourglass cylindrical detail within the gage section of the thin-walled tubular specimen.

ACKNOWLEDGMENT

The diligent efforts of Mr. Chris Burke in performing the high temperature axial-torsional fatigue tests are gratefully acknowledged.

REFERENCES

1. Brown, M.W., and Miller, K.J., "A Theory for Fatigue Failure under Multiaxial Stress-Strain Conditions," Proceedings, Institution of Mechanical Engineers, Vol. 187, No. 65/73, 1973, pp. 745–755.
2. E. Krempl., The Influence of State of Stress on Low-Cycle Fatigue of Structural Materials: A Literature Survey and Interpretive Report, ASTM STP 549, American Society for Testing and Materials, Philadelphia, 1974, pp. 1–46.
3. Garud, Y.S., "Multiaxial Fatigue: A Survey of the State of the Art," Journal of Testing and Evaluation, Vol. 9, No. 3, May 1981, pp. 165–178.
4. Miller, K.J., and Brown, M.W., "Multiaxial Fatigue: A Brief Review," Fracture 84, Proceedings of the Sixth International Conference on Fracture held in New Delhi, India, Pergamon Press, 1984, pp. 31–56.

5. Zamrik, S.Y., "An Investigation of Strain Cycling Behavior of 7075-T6 Aluminum Under Combined State of Strain: The Effects of Out-of-Phase, Biaxial Strain Cycling on Low Cycle Fatigue," NASA CR-72843, National Aeronautics and Space Administration, Washington, DC, January 1972, pp. 1–32.
6. Blass, J.J., and Zamrik, S.Y., "Multiaxial Low-Cycle Fatigue of Type 304 Stainless Steel," ASME-MPC Symposium on Creep-Fatigue Interaction, MPC-3, R.M. Curran, ed., The American Society of Mechanical Engineers, New York, December 1976, pp. 129–159.
7. Kanazawa, K., Miller, K.J., and Brown, M.W., "Low-Cycle Fatigue Under Out-of-Phase Loading Conditions," Journal of Engineering Materials and Technology, July 1977, pp. 222–228.
8. Socie, D.F., and Shield, T.W., "Mean Stress Effects in Biaxial Fatigue of Inconel 718," Journal of Engineering Materials and Technology, Vol. 106, July 1984, pp. 227–232.
9. Socie, D.F., Waill, L.A., and Dittmer, D.F., "Biaxial Fatigue of Inconel 718 Including Mean Stress Effects," Multiaxial Fatigue, ASTM STP 853, K.J. Miller and M.W. Brown, eds., American Society for Testing and Materials, Philadelphia, 1985, pp. 463–481.
10. Wu, H.C., and Yang, C.C., "On the Influence of Strain-Path in Multiaxial Fatigue Failure," Journal of Engineering Materials and Technology, Vol. 109, April 1987, pp. 107–113.
11. Socie, "Multiaxial Fatigue Damage Models," Journal of Engineering Materials and Technology, Vol. 109, October 1987, pp. 293–298.
12. Jones, D.J., and Kurath, P., "Cyclic Fatigue Damage Characteristics Observed for Simple Loadings Extended to Multiaxial Life Prediction," NASA CR-182126, National Aeronautics and Space Administration, Washington, DC, June 1988, pp. 1–93.
13. Fatemi, A., and Socie, D.F., "A Critical Plane Approach to Multiaxial Fatigue Damage Including Out-of-Phase Loading," Fatigue and Fracture of Engineering Materials and Structures, Vol. 11, No. 3, 1988, pp. 149–165.
14. Fatemi, A., and Kurath, P., "Multiaxial Fatigue Life Predictions Under the Influence of Mean-Stresses," Journal of Engineering Materials and Technology, Vol. 110, October 1988, pp. 380–388.
15. Fatemi, A., and Stephens, R.I., "Biaxial Fatigue of 1045 Steel Under In-Phase and 90 Deg Out-of-Phase Loading Conditions," Multiaxial Fatigue: Analysis and Experiments, AE-14, G.E. Leese and D. Socie, eds., Society of Automotive Engineers, Warrendale, PA, 1989, pp. 121–138.
16. Nitta, A., Ogata, T., and Kuwabara, K., "Fracture Mechanisms and Life Assessment Under High-Strain Biaxial Cyclic Loading of Type 304 Stainless Steel," Fatigue and Fracture of Engineering Materials and Structures, Vol. 12, No. 2, 1989, pp. 77–92.
17. Jayaraman, N., and Ditmars, M.M., "Torsional and Biaxial (Tension-Torsion) Fatigue Damage Mechanisms in Waspaloy at Room Temperature," International Journal of Fatigue, Vol. 11, No. 5, 1989, pp. 309–318.
18. Bonacuse, P.J., and Kalluri, S., "Results of Inphase Axial-Torsional Fatigue Experiments on 304 Stainless Steel," NASA TM–101464, National Aeronautics and Space Administration, Washington, D.C., March 1989, pp. 1–19.
19. Bonacuse, P.J., and Kalluri, S., "Axial-Torsional Fatigue: A Study of Tubular Specimen Thickness Effects," NASA TM–103637, National Aeronautics and Space Administration, Washington, D.C., December 1990, pp. 1–16.
20. Bonacuse, P.J. and Kalluri, S., "Elevated Temperature Axial and Torsional Fatigue Behavior of Haynes 188," NASA TM–105396, National Aeronautics and Space Administration, Washington, DC, June 1992.
21. Kalluri, S., and Bonacuse, P.J., "A Data Acquisition and Control Program for Axial-Torsional Fatigue Testing," Application of Automation Technology to Fatigue and Fracture Testing, ASTM STP 1092, A.A. Braun, N.E. Ashbaugh, and F.M. Smith, eds., American Society for Testing and Materials, Philadelphia, 1990, pp. 269–287.
22. "Case 1592-7," Cases of ASME Boiler and Pressure Vessel Code, American Society of Mechanical Engineers, New York, 1975, pp. 388–389.

23. Manson, S.S., and Halford, G.R., Discussion to the paper "Multiaxial Low Cycle Fatigue of Type 304 Stainless Steel" by J.J. Blass and S.Y. Zamrik., Journal of Engineering Materials and Technology, Vol. 99, No. 3, July 1977, pp. 283–285.
24. Davis, E.A., and Connelly, F.M., "Stress Distribution and Plastic Deformation in Rotating Cylinders of Strain-Hardening Material," Journal of Applied Mechanics, Transactions of the American Society of Mechanical Engineers, Vol. 81, 1959, pp. 25–30.
25. Smith, K.N., Watson, P., and Topper, T.H., "A Stress-Strain Function for the Fatigue of Metals," Journal of Materials, JMSLA, Vol. 5, No. 4, December 1970, pp. 767–778.
26. Lefebvre, D.F., Ameziane-Hassani, H., and Neale, K.W., "Accuracy of Multiaxial Fatigue Testing with Thin-Walled Tubular Specimens," Factors That Effect Precision of Mechanical Tests, ASTM STP 1025, R. Papirno and H.C. Weiss, eds., American Society for Testing and Materials, Philadelphia, 1989, pp. 103–114.

TABLE I.—MECHANICAL PROPERTIES OF HAYNES 188 AT 760 °C

	Axial property[a]	Shear property[a]
Monotonic stress-strain properties:		
Elastic modulus: E, G (GPa)	170.2	64.4
Elastic Poisson's ratio: ν_e	0.321	-------
Plastic Poisson's ratio: ν_p	0.5	-------
Yield strength, 0.2%: σ_y, τ_y (MPa)	268	163
Strength coefficient: K, K_t (MPa)	512	264
Strain hardening exponent: n, n_t	0.093	0.083
Percent reduction in area: %RA	55.1	-------
Ultimate tensile strength: σ_u (MPa)	490	-------
Cyclic stress-strain properties:		
Strength coefficient: K′, K_t' (MPa)	891	589
Strain hardening exponent: n′, n_t'	0.113	0.142
Fatigue life relation properties:		
Elastic exponent: b, b_t	−0.082	−0.100
Plastic exponent: c, c_t	−0.730	−0.715
Elastic coefficient: B, B_t	0.0091	0.0184
Plastic coefficient: C, C_t	0.590	2.17
Strength coefficient: σ_f', τ_f' (MPa)	823	635
Ductility coefficient: ε_f', γ_f'	0.489	1.78

[a]Data from reference 20.

TABLE II.—IN-PHASE AND OUT-OF-PHASE AXIAL-TORSIONAL FATIGUE DATA OF HAYNES 188 AT 760 °C

Specimen number	λ	ϕ, deg	$\Delta\varepsilon$	$\Delta\gamma$	$\Delta\sigma$, MPa	σ_o, MPa	$\Delta\tau$, MPa	τ_o, MPa	N_f
HY51	0.87	0	0.00963	0.00833	789	−4	227	−1	739
HY30	0.86		.00653	.00563	586	−3	357	−1	12 136
HY31	1.70		.01472	.02504	802	−1	427	1	310
HY26	1.71		.00815	.01393	668	−2	377	0	910
HY11	1.70		.00549	.00934	629	0	358	−1	1 906
HY10	1.69		.00408	.00689	566	4	331	−2	[a]6 261
HY9	1.67		.00306	.00510	510	10	304	−5	[a]18 517
HY28	1.69		.00240	.00406	432	38	261	−8	[b]255 536
HY35	3.48		.00657	.02285	443	−5	477	0	671
HY37	3.47		.00325	.01128	361	−3	419	0	2 929
HY50	1.79	30	.00390	.00698	586	−16	357	8	[a]12 136
HY54	1.80	60	.00387	.00698	624	2	375	1	[a]11 564
HY53	1.81	60	.00386	.00698	631	−4	380	1	[a]20 693
HY60	1.69	90	.01089	.01844	1013	−8	611	0	[c]393
HY65	1.73		.00806	.01393	964	−9	574	1	944
HY66	1.73		.00808	.01397	910	−10	544	0	[a]1 088
HY61	1.71		.00549	.00937	782	−6	453	1	2 270
HY38	1.76		.00440	.00776	726	−15	422	4	[d]4 624
HY68	1.75		.00448	.00782	727	−1	427	0	[a]9 264
HY56	1.77		.00394	.00697	666	−25	392	7	[a,d]10 524
HY46	1.75		.00393	.00689	674	8	415	3	[a]16 003
HY64	1.74		.00295	.00514	523	−75	338	23	[b]250 000

[a]Main crack that caused specimen failure was at an extensometer indentation.
[b]Specimen did not fail. Test was a runout.
[c]Specimen buckled slightly.
[d]Test was conducted with sinusoidal waveforms.

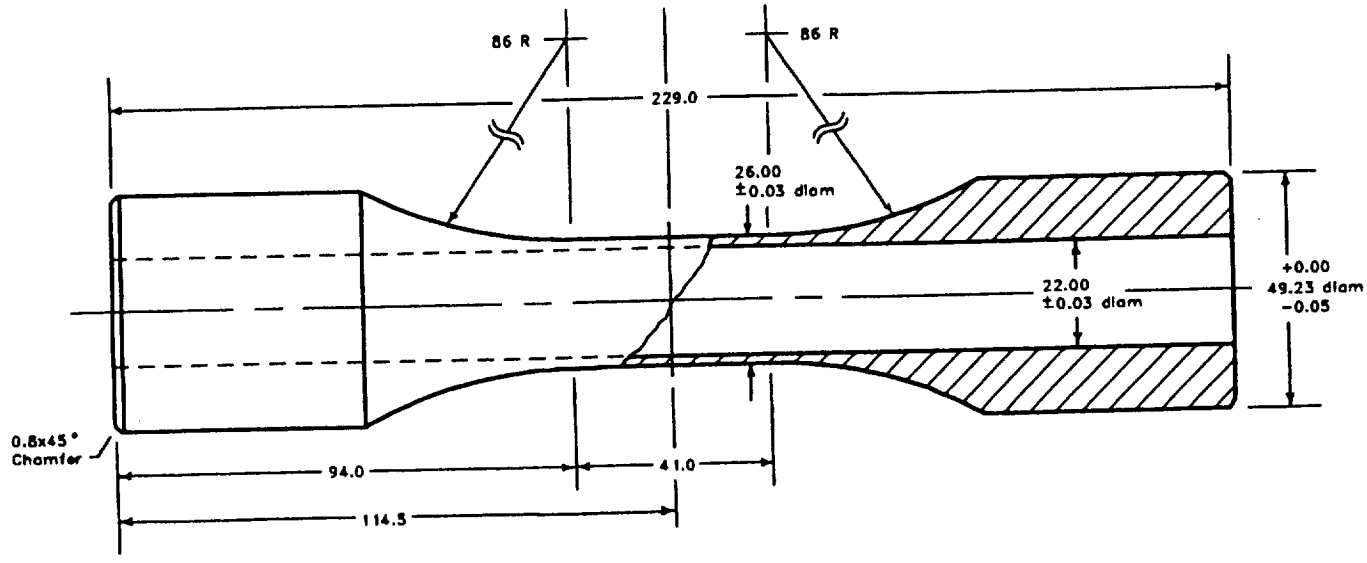

All dimensions are in millimeters.

Figure 1.—Geometry of the thin-walled tubular fatigue specimen.

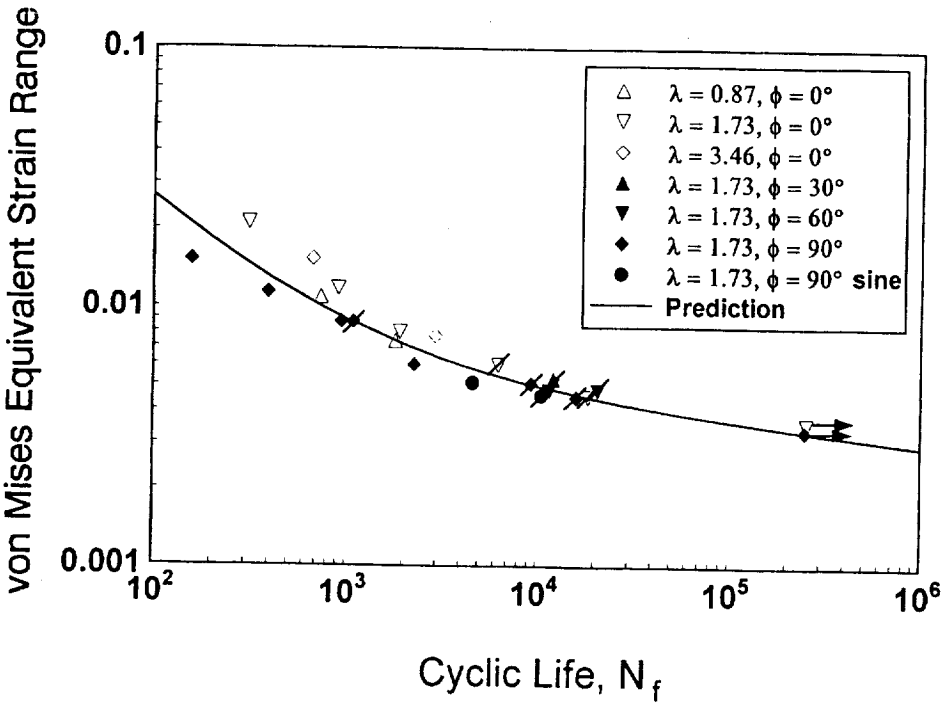

Figure 2.—Life prediction by the von Mises equivalent strain range model.

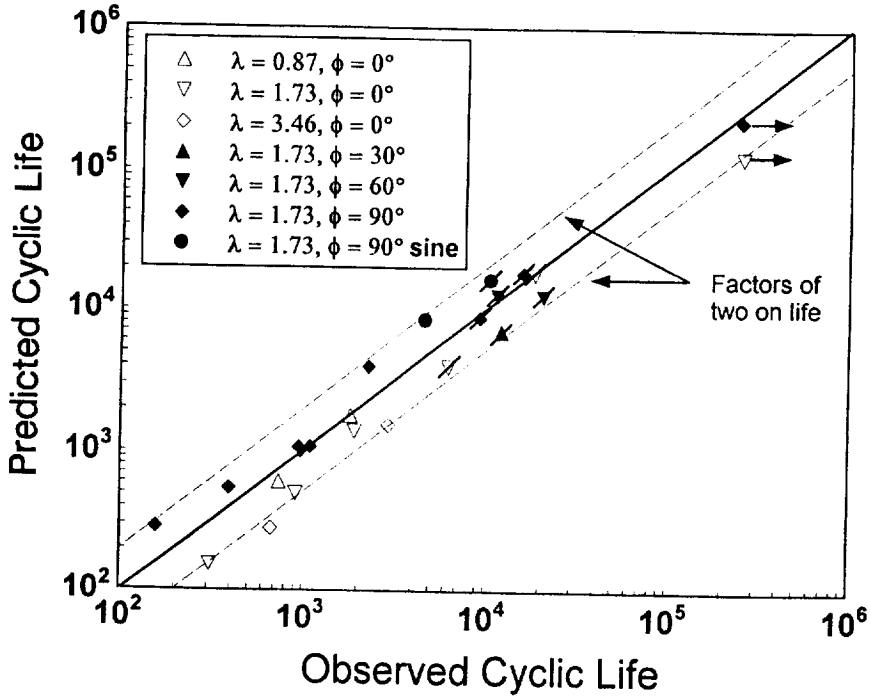

Figure 3.—Comparison of the observed and predicted lives by the von Mises equivalent strain range model.

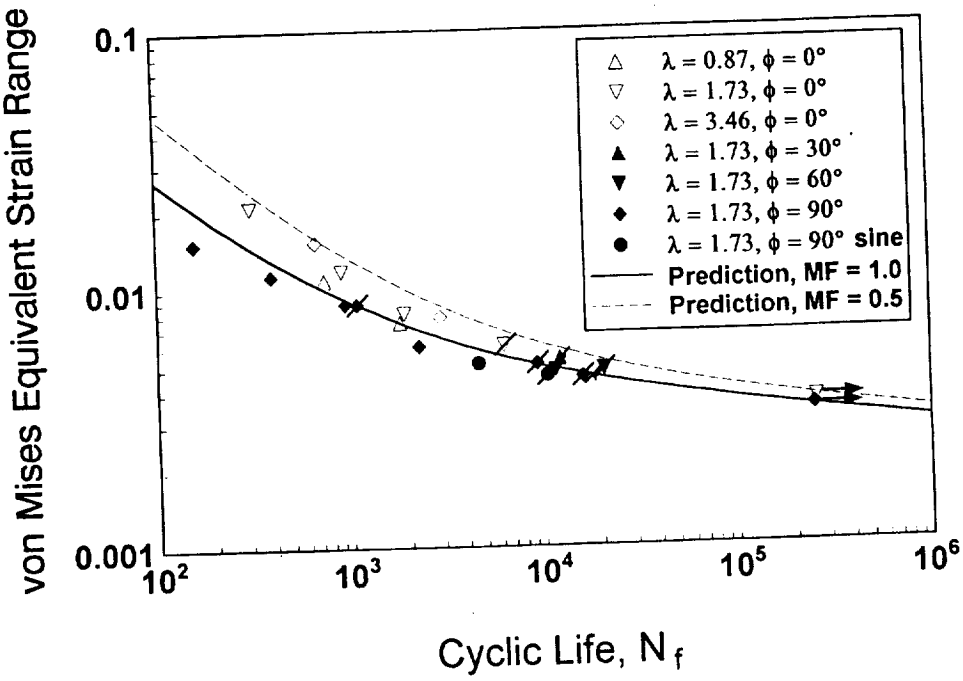

Figure 4.—Life prediction by the Modified Multiaxiality Factor Approach.

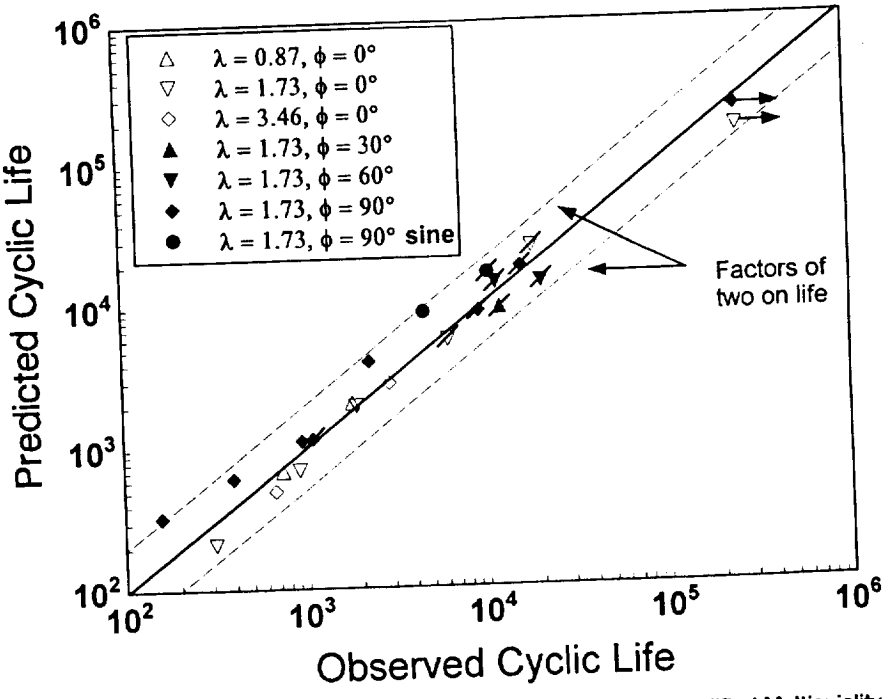

Figure 5.—Comparison of the observed and predicted lives by the Modified Multiaxiality Factor Approach.

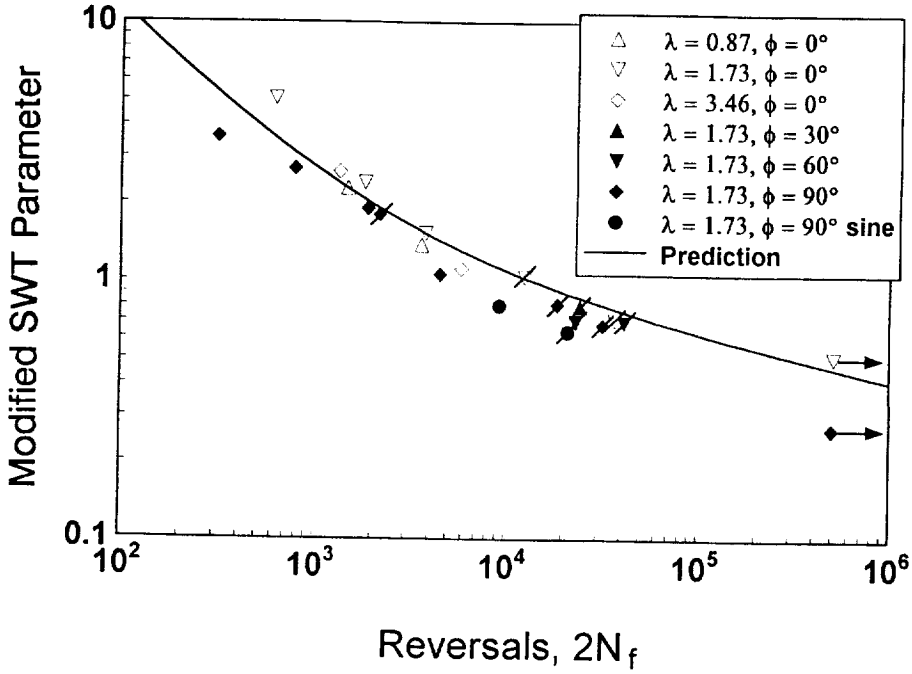

Figure 6.—Life prediction by the Modified Smith-Watson-Topper Parameter.

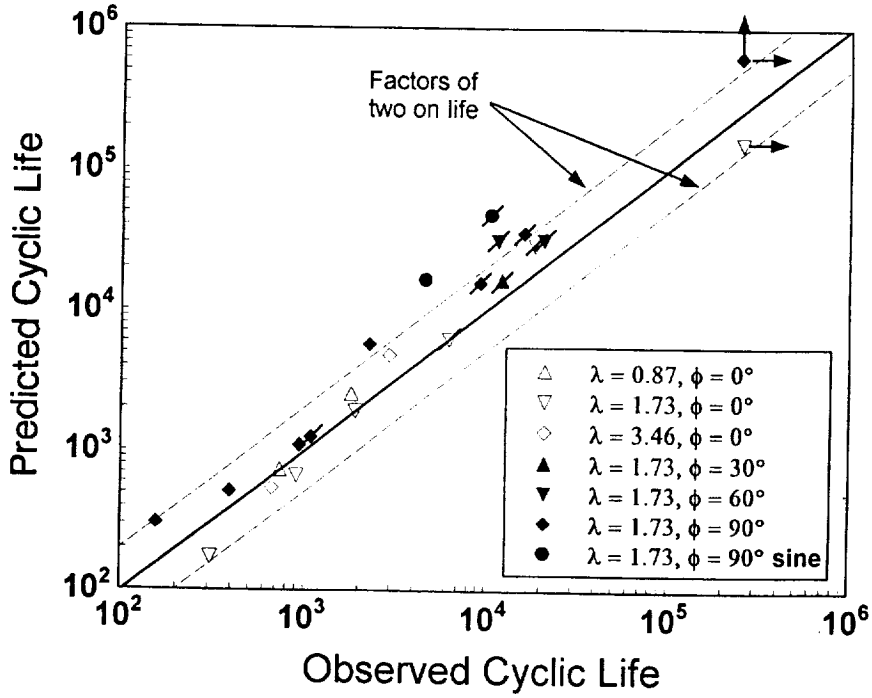

Figure 7.—Comparison of the observed and predicted lives by the Modified Smith-Watson-Topper Parameter.

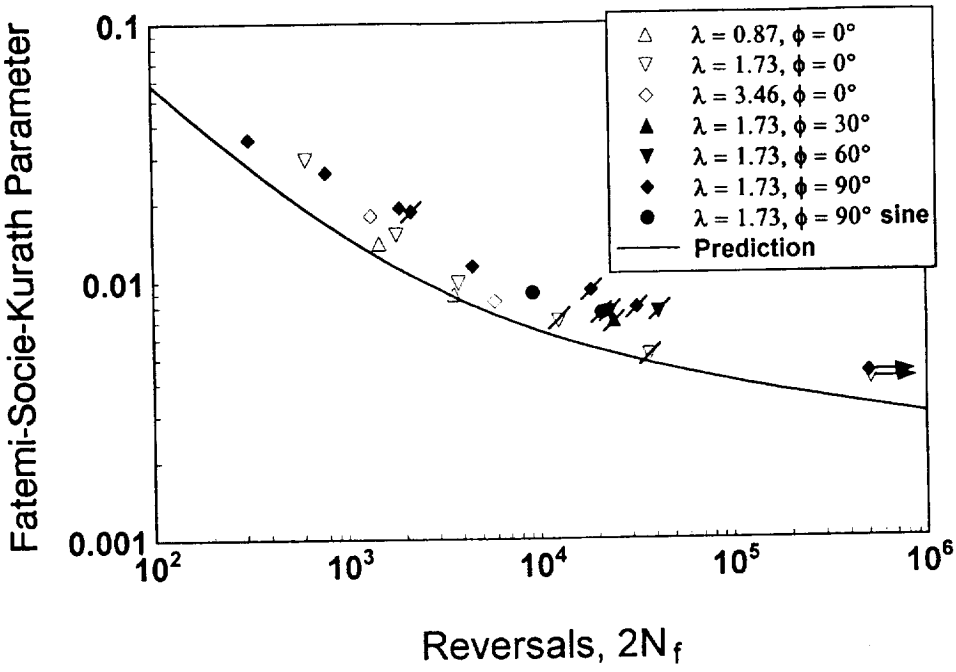

Figure 8.—Life prediction by the Fatemi-Socie-Kurath Model.

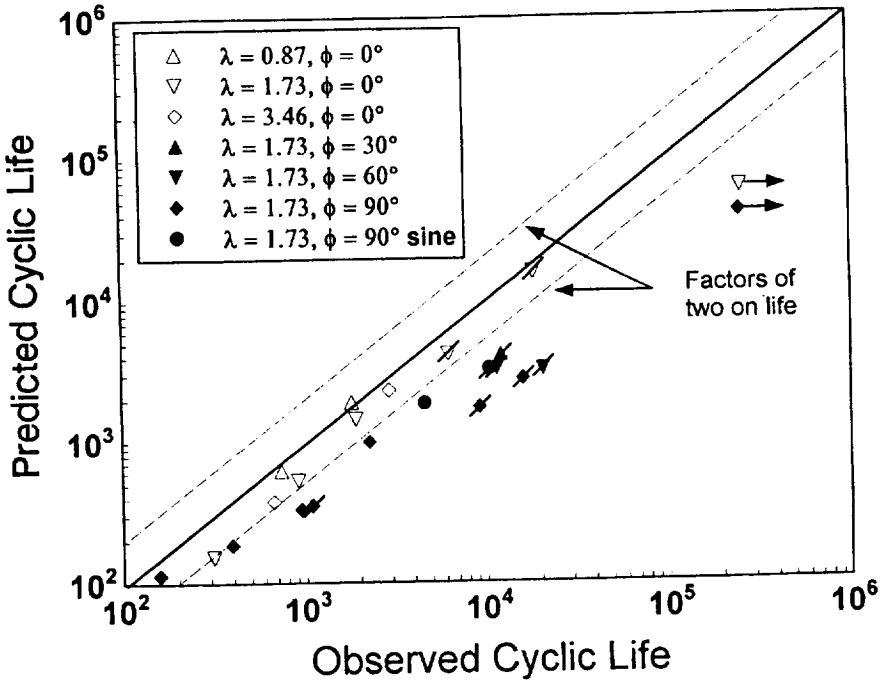

Figure 9.—Comparison of the observed and predicted lives by the Fatemi-Socie-Kurath Model.

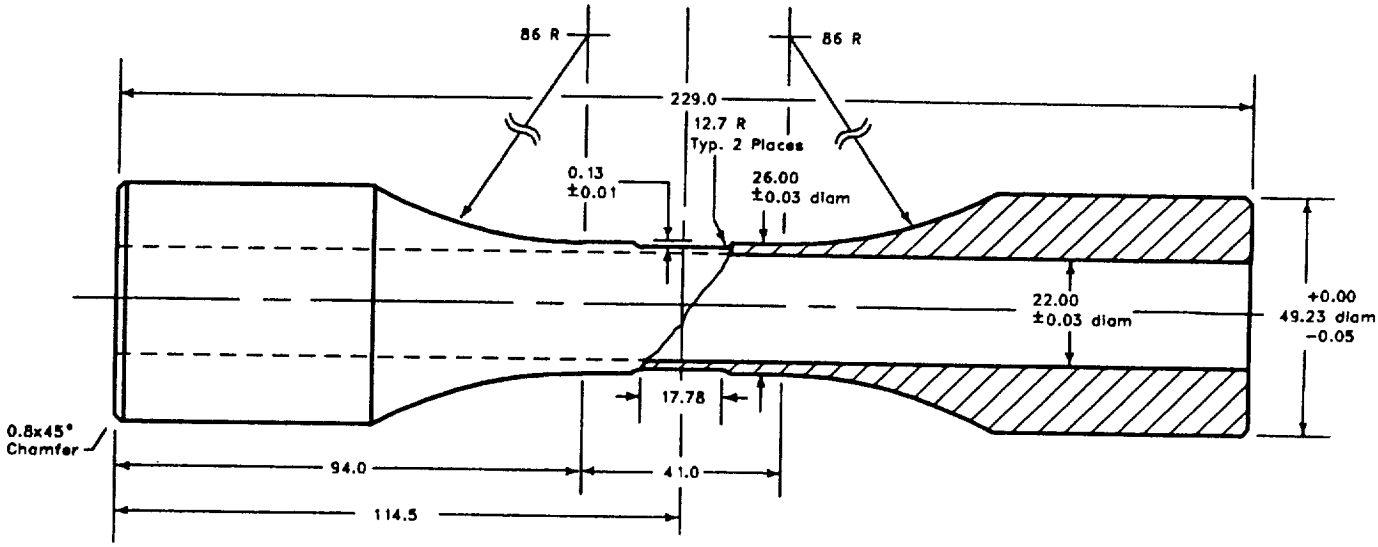

All dimensions are in millimeters.

Figure 10.—Thin-walled tubular specimen with a uniform cylindrical detail in the gage section.

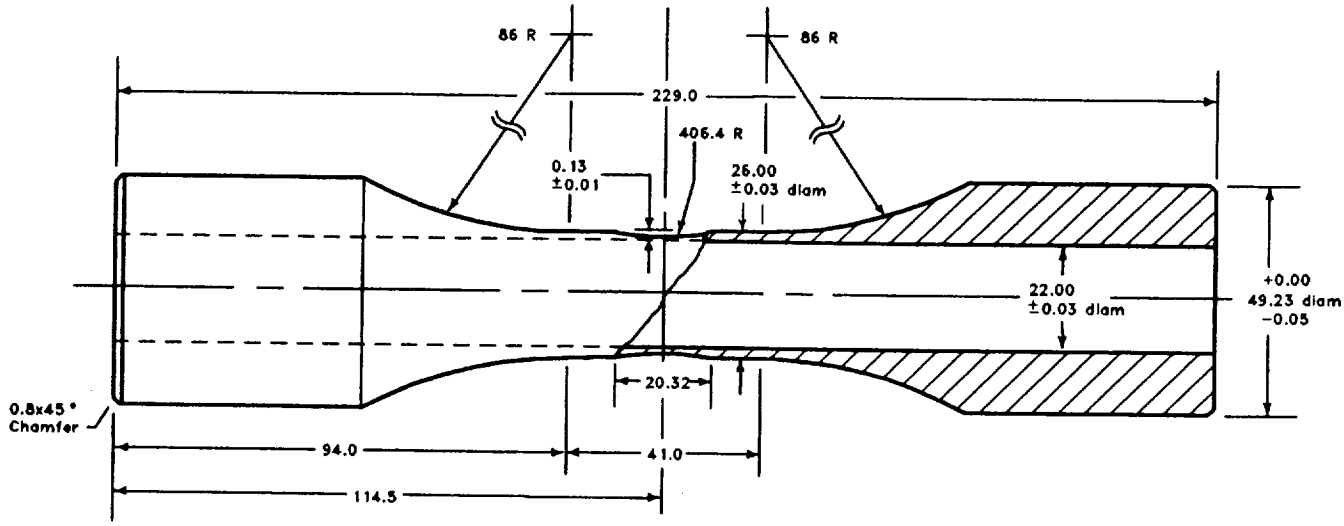

All dimensions are in millimeters.

Figure 11.—Thin-walled tubular specimen with an hourglass cylindrical detail in the gage section.